Elasto-plastic hemispherical contact models for various mechanical properties

J J Quicksall, R L Jackson and **I Green***
Georgia Institute of Technology, Atlanta, Georgia, USA

Abstract: This work uses the finite element technique to model the elastoplastic deformation of a hemisphere contacting a rigid flat for various material properties typical of aluminium, bronze, copper, titanium and malleable cast iron. Additionally, this work conducted parametric finite element method (FEM) tests on a generic material in which the elastic modulus and Poisson's ratio are varied independently while the yield strength is held constant. A larger spectrum of material properties are covered in this work than in most previous studies. The results from this work are compared with two previously formulated elastoplastic models simulating the deformation of a hemisphere in contact with a rigid flat. Both of the previously formulated models use carbon steel mechanical properties to arrive at empirical formulations implied to pertain to various materials. While both models considered several carbon steels with various yield strengths, they did not test materials with various Poisson's ratios or elastic moduli. The previously generated elastoplastic models give fairly good predictions when compared with the FEM results for various material properties from the current work, except that one model produces more accurate predictions overall, especially at large deformations where other models neglect important trends due to decreases in hardness with increasing deformation.

Keywords: asperity, Hertzian contact, hemispherical contact, contact mechanics, surface deformation, elastoplastic contact

NOTATION

A	area of contact
C	critical yield stress coefficient
e_y	ratio of yield strength to elastic modulus $= S_y/E$
E	elastic modulus
H	hardness
H_G	hardness geometric limit
K	hardness factor
P	contact force
R	radius of hemispherical asperity
S_y	yield strength
v	Poisson's ratio
ω	interference between the hemisphere and the surface

Superscripts

$'$	equivalent
$*$	dimensionless

Subscripts

c	critical value at the onset of plastic deformation
E	elastic regime
P	fully plastic regime
t	transitional value from elastic to elastoplastic behaviour

The MS was received on 17 October 2003 and was accepted after revision for publication on 4 June 2004.
* *Corresponding author: The George W. Woodruff School of Mechanical Engineering, Georgia Institute of Technology, Atlanta, Georgia 30332–0405, USA.*

1 INTRODUCTION

Contact between a deformable hemisphere and a rigid flat surface is commonplace in modelling many engineering applications. On a macroscopic scale, a ball bearing forced against the race of a bearing can be approximated by a hemisphere in contact with a rigid flat surface. On a microscopic scale, small asperities

modelled as hemispheres dispersed across two surfaces forced together constitute a similar form of contact (although actual asperities may have shapes differing greatly from this hemispherical approximation). The contact area and pressure between two surfaces is important on both scales. For the macroscopic scale, unacceptable deformations on a ball bearing may be the result of excessive load. For the microscopic scale, contact area between asperities affects friction, wear and conduction between two surfaces. General empirical approximations for relating contact area and contact force with hemisphere deformation are desired for accurate solutions to many engineering problems.

Many previous models have been formulated, such as the Zhao–Maletta–Chang [**1**] and Chang–Etsion–Bogy (CEB) [**2**] models, but recent findings have proven them to be inadequate [**3**, **4**]. Thus these models will not be considered in this work.

Recently, two independent studies by Jackson and Green (JG) [**3**] and Kogut and Etsion (KE) [**4**] have utilized the finite element method (FEM) to model hemispherical contact with a rigid flat. Both models use the Hertz solution [**5**] to non-dimensionalize their results for interference, contact area and contact force (see the Appendix), so that these non-dimensional values equal unity at the onset of yielding. The models simulate deformation of carbon steels to arrive at empirical formulations for non-dimensional contact area and contact force. The formulations imply that they are applicable to all ductile materials, but the carbon steels modelled to create them have fixed values of Poisson's ratio and modulus of elasticity. The present work utilizes the FEM to conduct similar deformation tests of a hemisphere in contact with a rigid flat, but it considers material properties typical of five other unique metals: aluminium, bronze, copper, titanium and malleable cast iron. Additionally, this work conducts parametric FEM tests on a generic material for which Poisson's ratio and the elastic modulus are independently varied. Neither this work nor the JG model created consider strain hardening in their analysis and, although KE investigated strain hardening, their model does not include it either. The objective of this work is to compare the empirical formulations proposed by JG and KE, as they apply to various sets of Poisson's ratio and elastic modulus typical of a wide variety of materials, with the results of this FEM study.

Both JG and KE modelled the frictionless contact of an elastic–perfectly plastic hemisphere pressed against a rigid flat by some specified distance known as the interference (Fig. 1). The hemisphere is described as elastic–perfectly plastic because at low interferences a high-stress region starts to form below the contact interface. Eventually the material yields in this high-stress region and a plastic core forms. The plastic core is surrounded by elastic material, which diminishes as the hemisphere is subjected to larger interferences. At higher interferences the plastic core expands in a three-dimensional fashion to the surface, and also inwards towards the centre of the hemisphere. The reason that the plastic region expands is because the material in the hemisphere that is flowing plastically can no longer resist additional load. Therefore, any additional load is carried by the surrounding elastic regions. At a value of ω^* between six and ten the plastic core reaches the surface near the edge of contact. Then there is an elastic core below the contact area that is surrounded by plastically deforming material. At a much higher load, anywhere within $68 \leqslant \omega^* \leqslant 110$ (depending on the material properties), the plastic region covers the entire contact area and occupies a large portion of the space in the hemisphere. This is known as the fully plastic regime. Through a large range of applied interferences the hemisphere deformation is subject to fully elastic, elastoplastic and fully plastic behaviours. JG and KE calculated non-dimensional contact area and force for an applied interference using the FEM. They then fitted empirical formulations to the resulting non-dimensional contact area and force as functions of non-dimensional interference and material properties. Because of the changing contact geometry and the transition from elastic to plastic behaviour, the non-dimensional contact area and force between a rigid flat and a hemisphere is not linearly related to the non-dimensional interference. While for the fully plastic regime KE assumed a fixed ratio of hardness to yield strength, JG found that the average contact pressure (i.e. 'hardness') varied with the deformed contact geometry, a result consistent with that obtained by Mesarovic and Fleck [**6**]. It should be noted that the term hardness as used in this work relates to a

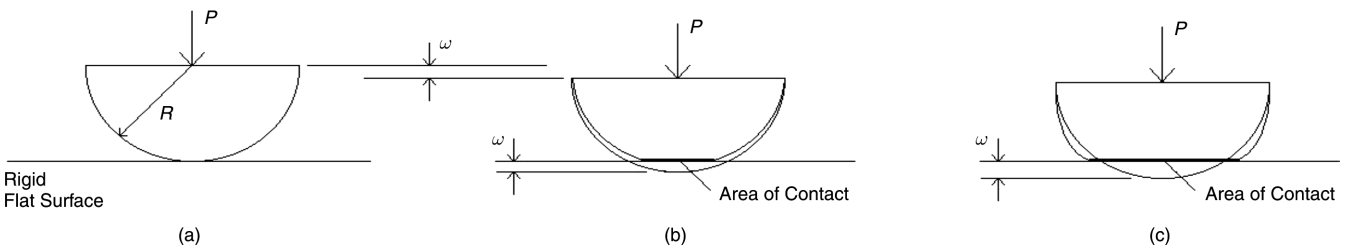

Fig. 1 Spherical contact model (a) before contact, (b) during mostly elastic deformation and (c) during mostly plastic deformation

deformable hemisphere in contact with a rigid flat unlike typical hardness tests where the hemisphere is considered rigid and the flat deformable. Other major differences between the JG and KE models are as follows:

1. As mandated by mesh convergence the mesh used by JG is at least an order of magnitude finer than that used by KE (the mesh by JG is also used in this work).
2. The deformation in the JG model continues to more than twice the deformation in the KE model.
3. The empirical formulations produced by the KE model use a piecewise fit that contains discontinuities at six times the critical interference, whereas the JG fit is continuous throughout.
4. The KE model assumes a truncation model beyond 110 times the critical interference (see the Appendix, equations (21) and (22) while the JG model does not. [The truncation model has been used by various researchers in the field (see, for example, references [**1**, **2**, **4**] and [**7**]). It has been extracted perhaps unsuitably from the work by Abbott and Firestone [**8**] who never made any suggestions about load or mean pressure; they simply assumed that progressive wear would truncate the surface height distribution. Hence, from this point forward the truncation model will be referred to without attributing it to Abbott and Firestone [**8**].]
5. The critical interference used by KE is based on a fixed relationship between hardness and yield strength (as if hardness is a material property), where the critical interference derived by JG does not rely on such a relationship at all. These differences are now detailed mathematically.

The KE solution applies for non-dimensional interferences between $\omega^* = 1$ and $\omega^* = 110$. It assumes the Hertz solution for $\omega^* < 1$, and the truncation model for $\omega^* > 110$. KE formulated piecewise non-dimensional contact area and contact force as follows: for $1 \leqslant \omega^* \leqslant 6$

$$\begin{aligned} P^*_{\mathrm{KE}} &= 1.03(\omega^*)^{1.425} \\ A^*_{\mathrm{KE}} &= 0.93(\omega^*)^{1.136} \\ \left(\frac{P}{AS_{\mathrm{y}}}\right)_{\mathrm{KE}} &= 1.19(\omega^*)^{0.289} \end{aligned} \tag{1}$$

and, for $6 \leqslant \omega^* \leqslant 110$,

$$\begin{aligned} P^*_{\mathrm{KE}} &= 1.40(\omega^*)^{1.263} \\ A^*_{\mathrm{KE}} &= 0.94(\omega^*)^{1.146} \\ \left(\frac{P}{AS_{\mathrm{y}}}\right)_{\mathrm{KE}} &= 1.61(\omega^*)^{0.117} \end{aligned} \tag{2}$$

In equation (1) note that at $\omega^* = 1$ the model is disjointed from the Hertz solution; the force is overestimated by 3 per cent while the area is underestimated by 7 per cent. Note also that equations (1) and (2) are disjointed at $\omega^* = 6$. Beyond $\omega^* = 110$ the contact hemisphere is assumed to be well into the fully plastic regime, and at this point the truncation model is assumed, where equation (2) does not asymptotically approach the truncation model, it merely intersects with it.

The JG model finds that contact area increases beyond the truncation model for interferences in the fully plastic regime. JG formulated nondimensional contact area for $\omega^* \geqslant 1.9$ as

$$A^* = \omega^* \left(\frac{\omega^*}{1.9}\right)^B \tag{3}$$

where

$$B = 0.14 \exp(23 e_{\mathrm{y}}) \tag{4}$$

$$e_{\mathrm{y}} = \frac{S_{\mathrm{y}}}{E'} \tag{5}$$

A geometric limit to hardness as explained in detail by JG is calculated to be

$$\frac{H_{\mathrm{G}}}{S_{\mathrm{y}}} = 2.84\left[1 - \exp\left(-0.82\left(\frac{a}{R}\right)^{-0.7}\right)\right] \tag{6a}$$

where a is the radius of the contact patch of the deformed hemisphere and R is the nominal radius of the hemisphere. Here the hardness changes as a function of a/R, or with the evolving geometry of contact. The trend may be explained by the progression schematically shown in Fig. 2. As the interference increases and the contact geometry changes, the limiting ratio $H_{\mathrm{G}}/S_{\mathrm{y}}$ of average pressure to yield strength must change from Tabor's predicted value of three to a theoretical value of one when $a = R$. It should be noted that equation (6a) is only valid for $0 < a/R \leqslant 0.412$, where

$$\frac{a}{R} = \frac{\pi C e_{\mathrm{y}}}{2}\left[\omega^*\left(\frac{\omega^*}{\omega^*_t}\right)^B\right]^{1/2} \tag{6b}$$

and is derived from equation (3) in the paper by JG. Caution should thus be taken when using equation (6a) outside this range. This range is acceptable for many applications, particularly tribological applications where

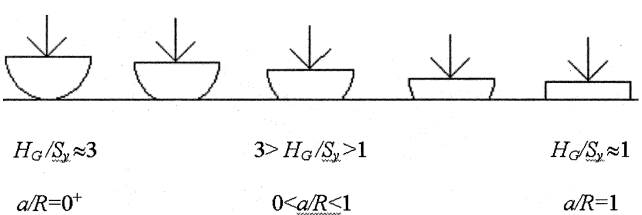

Fig. 2 Diagram of progression of change in hardness with geometry

deformations above this range are either unlikely or unacceptable. By substituting equation (6b) into equation (6a) Jackson and Green found that

$$\frac{H_G}{S_y} = 2.84\left[1 - \exp\left(-0.82\left(\frac{\pi C e_y}{2}\sqrt{\omega^*}\left(\frac{\omega^*}{1.9}\right)^{B/2}\right)^{-0.7}\right)\right] \tag{6c}$$

where H_G is the hardness geometric limit and C is the critical yield stress coefficient [equation (13)]. Equation (6c) incorporates the effect that the deformed geometry has on hardness, which is defined as average contact pressure. JG found that the ratio H_G/S_y for fully plastic yielding approaches 2.84. Using equation (6c), the JG model calculates the non-dimensional contact force for $\omega^* \geqslant 1.9$ as

$$P^* = \left[\exp\left(-\frac{1}{4}(\omega^*)^{5/12}\right)\right](\omega^*)^{3/2} + \frac{4H_G}{CS_y}\left[1 - \exp\left(-\frac{1}{25}(\omega^*)^{5/9}\right)\right]\omega^* \tag{7}$$

For $\omega^* < 1.9$, the JG model assumes the Hertz solution. Theoretically the Hertz solution is valid only up to $\omega^* = 1$. However, the FEM results obtained by JG find that the Hertz solution can be extended to $\omega^* < 1.9$ without a noticeable sacrifice in accuracy. This is probably due to the fact that, although plastic deformation does form at $\omega^* = 1$ and beyond, it is small enough and contained in a predominantly elastic region. The JG formulation for non-dimensional contact area and contact force provides continuous functions throughout the entire range of deformation, $0 \leqslant \omega^* \leqslant 250$.

2 PROCEDURE

The validity of the empirical formulations for contact with an elastoplastic hemisphere presented by the KE and the JG models is tested by conducting the FEM of hemispherical contact with varied material properties. Two sets of tests were conducted using an FEM similar to that used by JG (who detailed the numerical procedure and convergence of the FEM). The first test generated contact area and contact force data for five hypothetical metals with Poisson's ratios, yield strengths and elastic modulus typical of aluminium, bronze, copper, titanium and malleable cast iron (see Table 1 for material properties). Non-dimensional interferences between $\omega^* = 5$ and $\omega^* = 250$ were used to generate data in both the elastoplastic and the fully plastic regimes, except for 'aluminium' at $\omega^* = 250$ and 'malleable cast iron' above $\omega^* = 10$ because of difficulties in obtaining solution convergence at these interferences.

Table 1 Material properties

Material	ν	S_y (GPa)	E (GPa)
Aluminium 7075-T6*	0.33	0.505	72
Bronze SAE 40*	0.33	0.125	93
Copper UNS C15500*	0.34	0.124	115
Titanium IMI 834*	0.31	0.925	120
Malleable cast iron typical†	0.25	0.250	170
Carbon steel†	0.32	0.210	200

*matweb.com.
† From reference [9].

The second set of tests generated non-dimensional contact area and contact force data for a generic material in which the elastic modulus and Poisson's ratio were independently varied with the yield strength held constant at $S_y = 200$ MPa. Firstly, Poisson's ratio was varied between 0.28 and 0.36 with the elastic modulus held constant at 200 GPa. Then, the elastic modulus was varied between 160 and 240 GPa with Poisson's ratio held constant at 0.32. The non-dimensional interference was set at $\omega^* = 20$, 80 and 250 for each test iteration.

The FEM used in this work is similar to that used by JG. The mesh consists of a minimum of 11 100 elements and may increase depending on the expected region of contact. The contact region is meshed by 100 contact elements. The non-dimensional area is calculated by finding the number of elements that form the radius of a contact patch. Some small error exists due to the resolution of a single contact element. The error due to contact patch resolution measuring the contact radius ranges from as much as 1.9 per cent for 'cast iron' at $\omega^* = 2$ to as little as 0.8 per cent for 'bronze' at $\omega^* = 250$.

3 NUMERICAL RESULTS

The relative difference between the models and the FEM conducted in this study is referred to as the percentage error and calculated as

$$\text{Percentage error} = 100\left(\frac{\text{model} - \text{FEM}}{\text{FEM}}\right)$$

For the first test modelling the deformation of five hypothetical materials the average error for the JG formulations is 3.10 per cent for non-dimensional contact area and 4.49 per cent for non-dimensional contact force. The average error for the KE model is 5.26 per cent for non-dimensional contact area and 7.34 per cent for the non-dimensional contact force. It should be noted that the KE model assumes the truncation

model above $\omega^* = 110$. The truncation model is used when calculating the average errors for the KE model at $\omega^* = 250$. The higher average error associated with the KE model's prediction of non-dimensional contact force is mostly due to the large error associated with truncation model values assumed at $\omega^* = 250$ (see the Appendix, equations (21) and (22)).

The second set of tests is conducted by first independently varying Poisson's ratio and then independently varying the elastic modulus for a generic material and was run using non-dimensional interferences of $\omega^* = 20,\ 80$ and 250. For this test, the KE model has a slightly lower average error for non-dimensional contact area than the JG model, and the JG model has a slightly lower average error for non-dimensional contact force than the KE model. Both models have average errors below 3.0 per cent for contact area and contact force.

Tests performed by holding Poisson's ratio constant at 0.32 and varying the elastic modulus also yield small errors for the JG and KE formulations. Again, the KE model has slightly lower average error for non-dimensional contact area, and the JG model produces a slightly lower average error for non-dimensional contact force. Neither model has an average error greater than 3.3 per cent for either non-dimensional contact force or non-dimensional contact area.

4 DISCUSSION

Figures 3 and 4 show the errors from tests conducted on various hypothetical materials. Generally, comparing the JG and KE models with the FEM results from this study reveals small errors for most tests. Nearly all results fall below 10 per cent error, and most results fall below 5 per cent error. There is a general trend for the errors of both the JG and the KE formulations to decrease with higher non-dimensional contact interference (except for the fully plastic case for the KE model in which the truncation model value is assumed). This is probably due to the increased accuracy of the FEM at higher interferences because the relative uncertainties of nodal position are higher at lower displacements. The JG formulations have an average error about 2 per cent less than the KE average error for both non-dimensional contact area and non-dimensional contact force. Part of this reduced error may be attributed to the higher number of degrees of freedom incorporated into the JG curve fit, the finer mesh used in the JG FEM than the KE FEM, and the similarity between the JG mesh and the mesh used in this model. Additionally, the JG model incorporates the changing hardness of the deforming hemisphere into its non-dimensional contact force formulations while the KE model assumes that the ratio of hardness to yield strength is fixed. For some

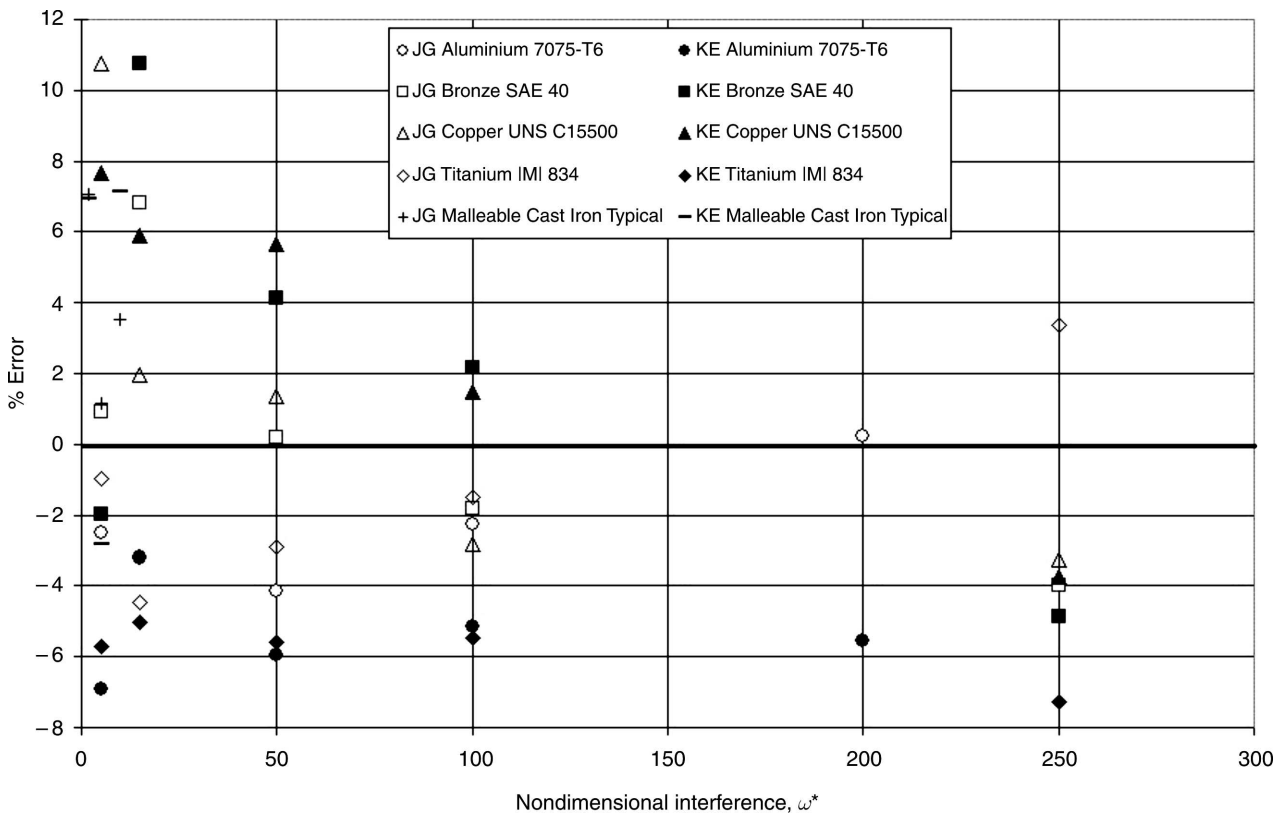

Fig. 3 Error of non-dimensional area as a function of non-dimensional interference between current FEM and values from JG and KE models

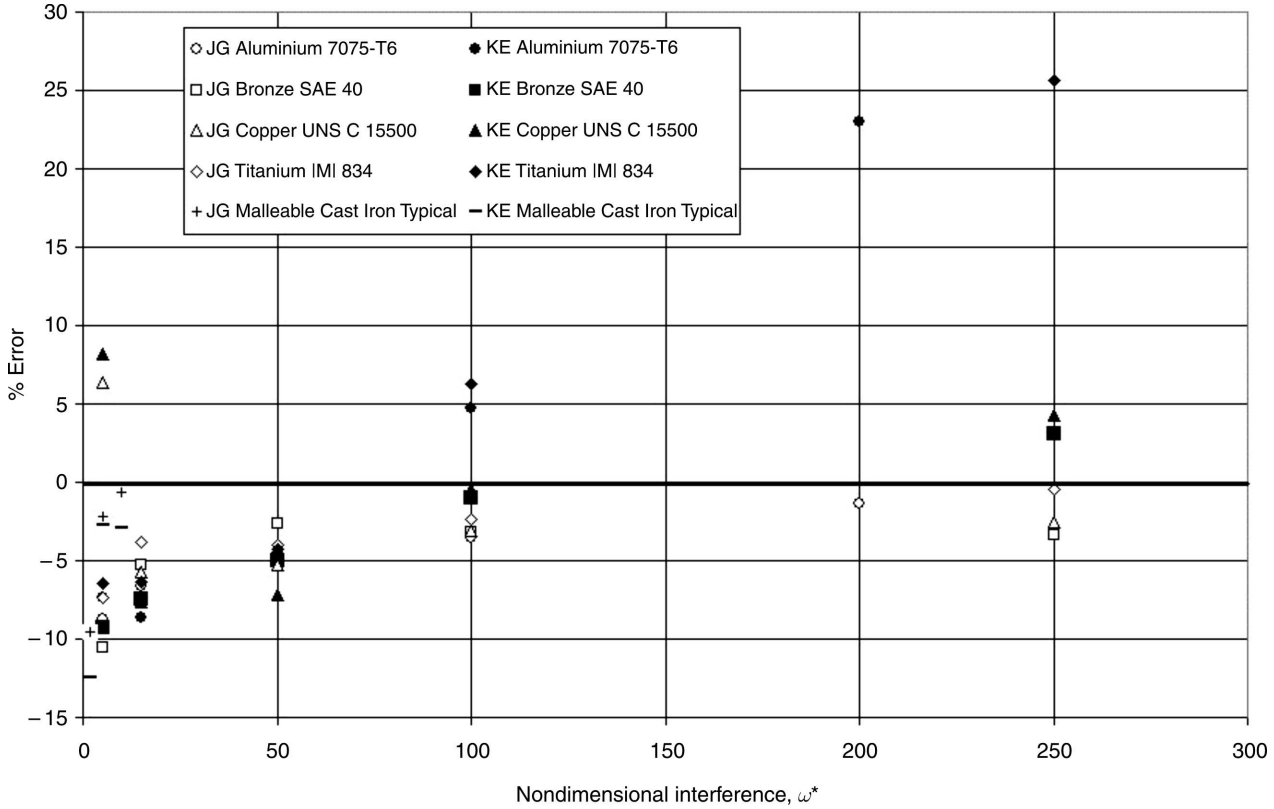

Fig. 4 Error of non-dimensional force as a function of non-dimensional interference between current FEM and values from JG and KE models

materials, e.g. 'aluminium' or 'titanium', the errors in the truncation model are significant (above 20 per cent) at large interferences. In Figs 3 and 4 it can be seen that generally the open symbols of JG are closer to zero than the full symbols of KE.

Errors for both models are even lower for the parametric tests which varied Poisson's ratio and elastic modulus independently for a generic material ($S_y = 200\,\text{MPa}$). Figures 5 and 6 show the errors for non-dimensional contact area and contact force when varying Poisson's ratio and holding the elastic modulus constant. The FEM conducted in the current work shows that the non-dimensional contact area increases with increasing Poisson's ratio at a non-dimensional interference of $\omega^* = 250$. The FEM results also show a dependence of the normalized load P^*, on Poisson's ratio (Fig. 7). At small interferences of $\omega^* = 20$ and $\omega^* = 80$ the dependence of P^* on v is weak, however, at interferences of $\omega^* = 250$, P^* decreases with increasing v. The JG model captures these trends while the KE model assumes that there is no dependence between P^* and v, although the errors of the KE model are still less than the JG model at some values of ω^* and v.

Finally, Fig. 8 shows the error of the JG and the KE models when Poisson's ratio is held constant at 0.32, and the elastic modulus is varied. The FEM results from this study indicate that non-dimensional contact area decreases slightly with increased elastic modulus, and non-dimensional contact force increases with increased elastic modulus. These trends are captured by the JG model but not by the KE model, although again there are some values of ω^* and E for which the KE model has smaller error.

5 CONCLUSION

This work presents the results of elastic–perfectly plastic hemispherical contact for a variety of material properties. These results are compared with the empirical formulations by JG and KE. Both the JG and the KE studies created formulations dependent on material properties without testing their models on materials with varied Poisson's ratio and elastic modulus. This work verifies these formulations against an FEM that did test varied material properties. Both sets of formulations show small relative errors compared with the FEM results of this test. These low errors offer an acceptable range of uncertainty for most engineering applications. The KE formulations are each segmented into two regions, with a discontinuity at each intersection, while the JG formulations are continuous. This may be advantageous when these equations need to be

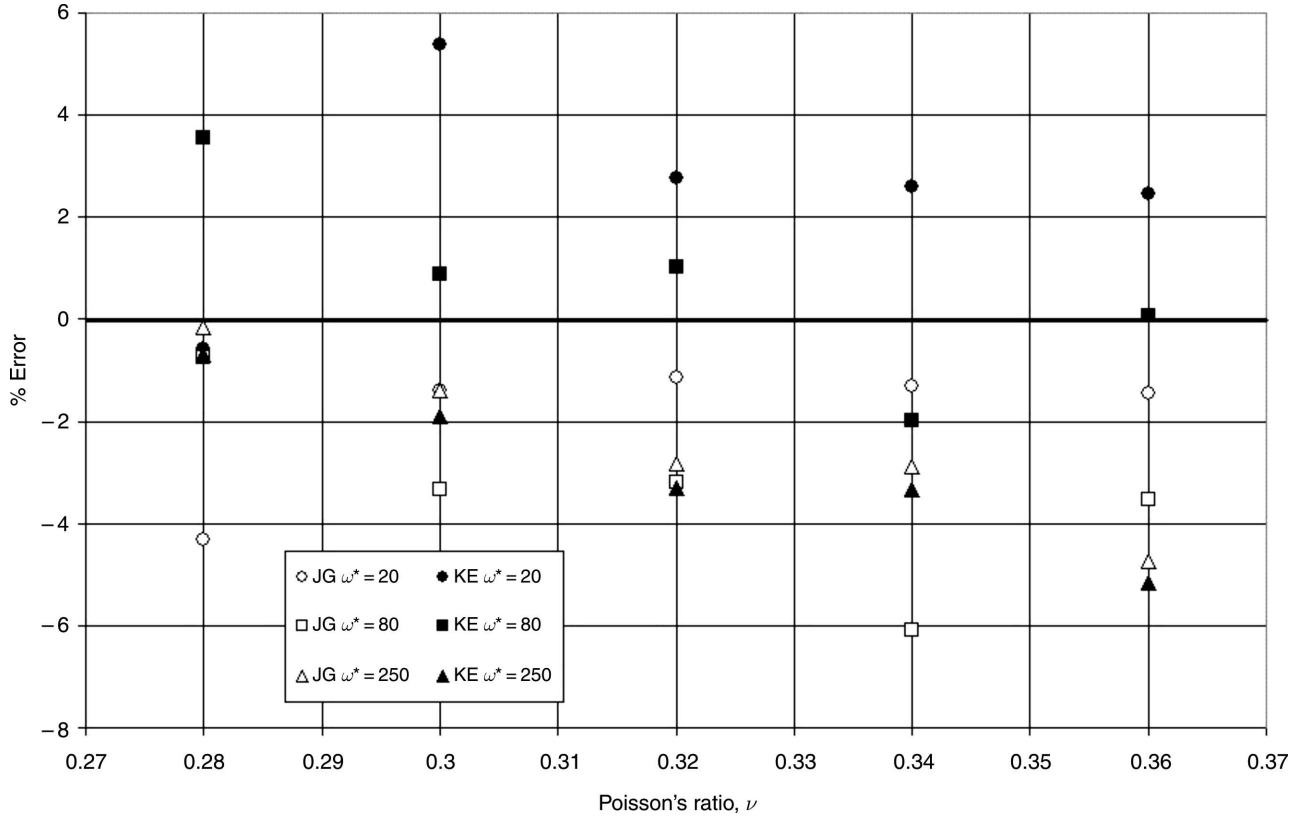

Fig. 5 Error of non-dimensional area as a function of Poisson's ratio between current FEM and values from JG and KE models

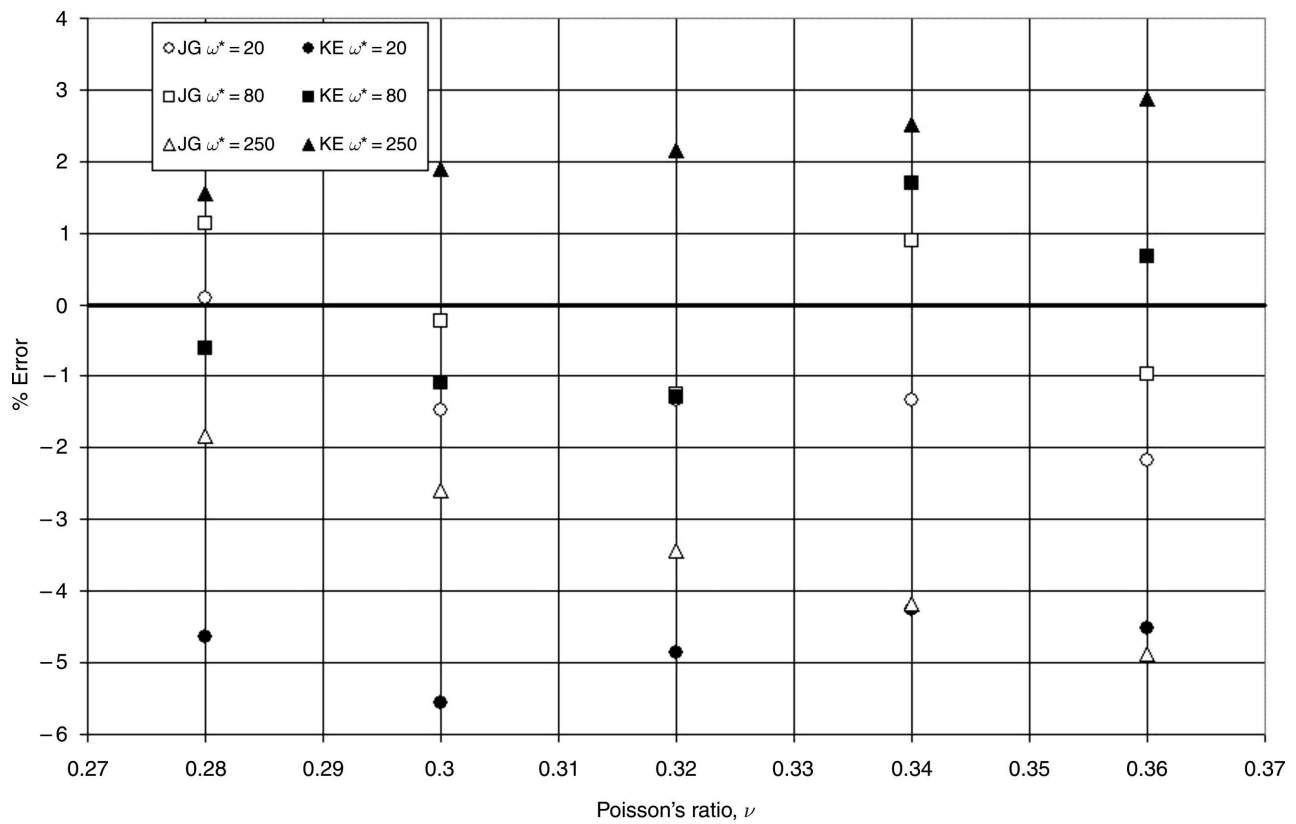

Fig. 6 Error of non-dimensional force as a function of Poisson's ratio between current FEM and values from JG and KE models

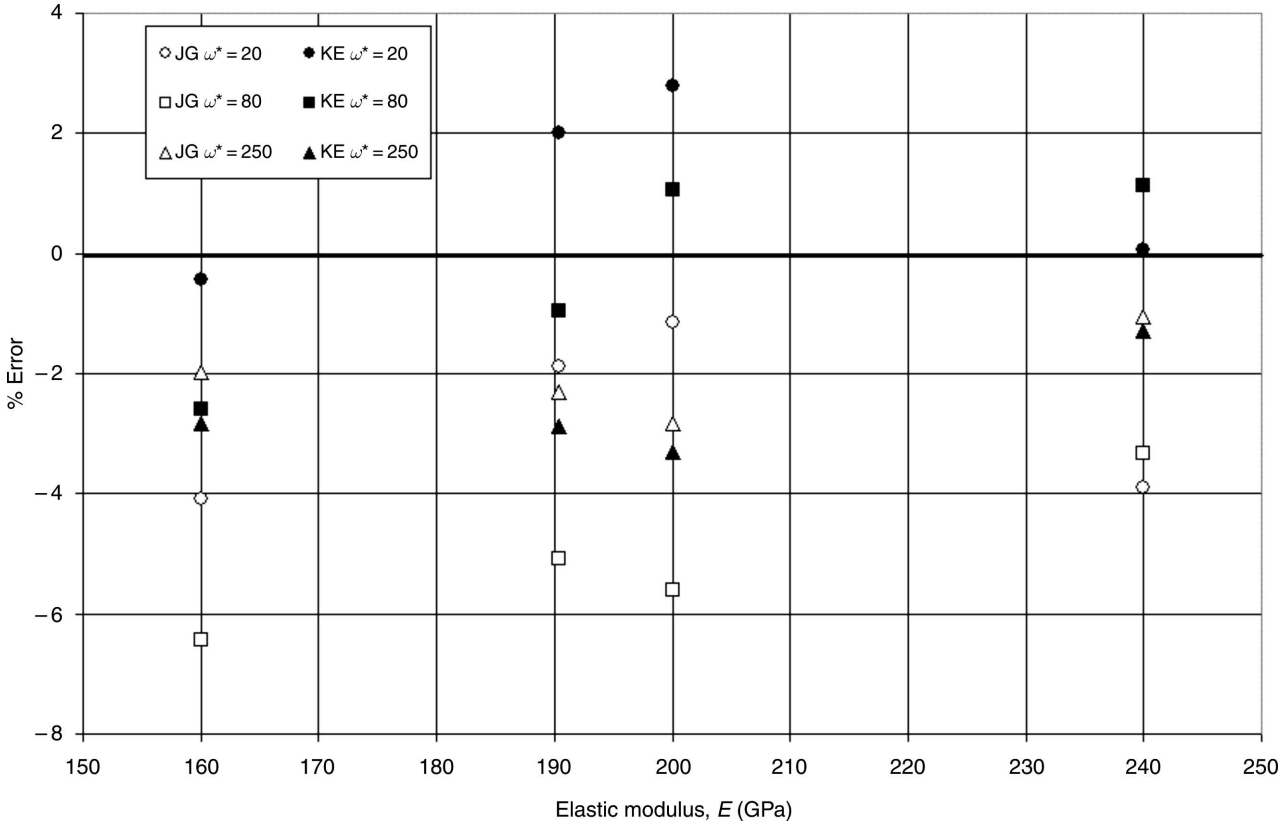

Fig. 7 Error of non-dimensional area as a function of elastic modulus between current FEM and values from JG and KE models

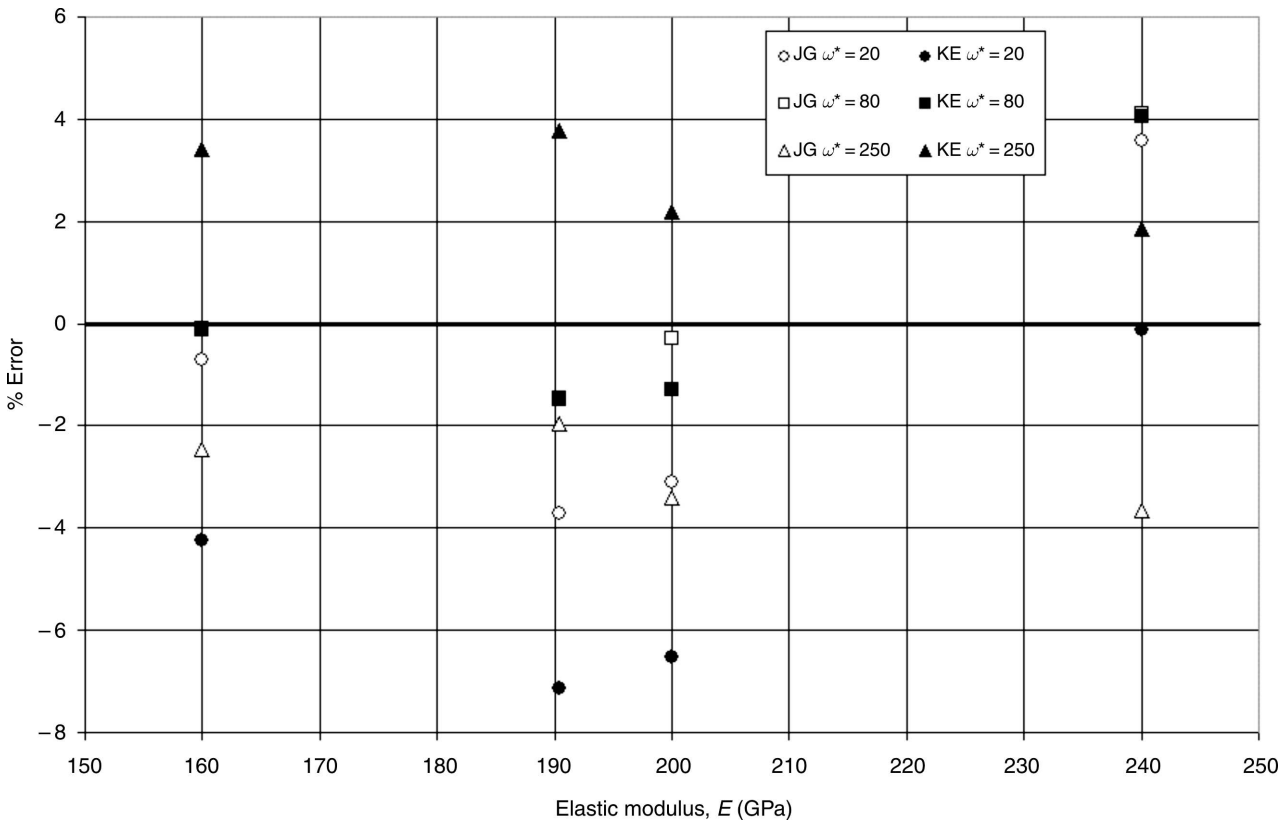

Fig. 8 Error of non-dimensional force as a function of elastic modulus between current FEM and values from JG and KE models

integrated, such as using the Greenwood–Williamson [**10**] integrals. For its continuity the JG formulation is somewhat more complex compared with the KE formulation. Overall, however, the JG model has a slightly smaller error than the KE model when compared with the current FEM results. This work finds that at large interferences the errors in the truncation model postulated by KE are significant (above 20 per cent).

REFERENCES

1 **Zhao, Y., Maletta, D. M.** and **Chang, L.** An asperity microcontact model incorporating the transition from elastic deformation to fully plastic flow. *Trans. ASME, J. Tribology*, 2000, **122**, 86–93.
2 **Chang, W. R., Etsion, I.** and **Bogy, D. B.** An elastic–plastic model for the contact of rough surfaces. *Trans. ASME, J. Tribology*, **109**, 257–263.
3 **Jackson, R. L.** and **Green, I.** A finite element study of elasto-plastic hemispherical contact. In Proceedings of the 2003 ASME–STLE International Tribology Conference, Preprint 2003-TRIB268.
4 **Kogut, L.** and **Etsion, I.** Elastic–plastic contact analysis of a sphere and a rigid flat. *Trans. ASME, J. Appl. Mechanics*, 2002, **69**(5), 657–662.
5 **Timoshenko, S.** and **Goodier, J. N.** *Theory of Elasticity*, 1951 (McGraw-Hill, New York).
6 **Mesarovic, S. D.** and **Fleck, N. A.** Frictionless indentation of dissimilar elastic–plastic spheres. *Int. J. Solids Structs*, 2000, **37**, 7071–7091.
7 **Greenwood, J. A.** and **Tripp, J. H.** The contact of two nominally flat rough surfaces. *Proc. Instn Mech. Engrs*, 1971, **185**, 625–633.
8 **Abbott E. J.** and **Firestone, F. A.** Specifying surface quality—a method based on accurate measurement and comparison. *Mech Engr*, 1933, **55**, 569–572.
9 **Shigley, J. E.** and **Mischke, C. R.** *Mechanical Engineering Design*, 5th Edition, 1989 (McGraw-Hill, New York).
10 **Greenwood, J. A.** and **Williamson, J. B. P.** Contact of nominally flat surfaces. *Proc. R. Soc. Lond. A*, 1966, **295**, 300–319.
11 **Johnson, K. L.** *Contact Mechanics*, 1985 (Cambridge University Press, Cambridge).
12 **Tabor, D.** *The Hardness of Materials*, 1951 (Clarendon, Oxford).

APPENDIX

Although the Hertz solution is formulated for contact between two hemispheres, an equivalent modulus of elasticity and radius can be calculated to apply to contact between a hemisphere and a rigid flat [**5**]. The Hertz theory of elastic contact calculates the contact area and contact force during fully elastic contact:

$$A_{\mathrm{E}} = \pi R\omega \tag{8}$$

$$P_{\mathrm{E}} = \tfrac{4}{3}E'\sqrt{R}(\omega)^{3/2} \tag{9}$$

where A_{E} is the circular contact area, P_{E} is the total contact load and ω is the interference. E', the equivalent elastic modulus, and R, the equivalent radius, are calculated as

$$\frac{1}{E'} = \frac{1-\nu_2^2}{E_1} + \frac{1-\nu_2^2}{E_2} \tag{10}$$

$$\frac{1}{R} = \frac{1}{R_1} + \frac{1}{R_2} \tag{11}$$

where $E_1, \nu_1, R_1, E_2, \nu_2$ and R_2 are the elastic moduli, Poisson's ratios and radii of hemispheres 1 and 2 respectively. The Hertz solution approximates the contact hemisphere as a parabolic curve with the radius of curvature at the tip of the parabola equal to the radius of the contact hemisphere. It also assumes that the deformation (interference) of the contact hemisphere is much less than the radius of the hemisphere, and that no friction is present between the hemisphere and rigid flat.

The Hertz solution can be used to non-dimensionalize contact area and contact force outside the truly elastic regime by obtaining the interference at the inception of yielding. JG calculated interference at the onset of plastic yielding using the von Mises yield criterion as

$$\omega_{\mathrm{c}} = \left(\frac{C\pi S_{\mathrm{y}}}{2E'}\right)^2 R \tag{12}$$

where ω_{c} is the critical interference, R is the contact hemisphere radius, E' is the equivalent elastic modulus, S_{y} is the yield strength and C is a function given in the JG study as

$$C = 1.295\exp(0.736\nu) \tag{13}$$

The critical contact area at yielding, A_{c}, was found by JG by substituting the critical interference [equation (12)] into the Hertz solution for contact area [equation (8)]:

$$A_{\mathrm{c}} = \pi^3\left(\frac{CS_{\mathrm{y}}R}{2E'}\right)^2 \tag{14}$$

The critical contact force P_{c} was found by JG by substituting the critical interference [equation (12)] into the Hertz solution for contact force:

$$P_{\mathrm{c}} = \frac{4}{3}\left(\frac{R}{E'}\right)^2\left(\frac{C\pi S_{\mathrm{y}}}{2}\right)^3 \tag{15}$$

KE used a critical interference given by CEB:

$$\omega_c = \left(\frac{\pi KH}{2E'}\right)^2 R \tag{16}$$

Here a fixed ratio of hardness H to yield strength S_y is assumed, $H = 2.8S_y$, which results in the factor K, given as

$$K = 0.454 + 0.41\nu \tag{17}$$

The critical area and critical force are found by substituting the critical interference into the Hertz solution. Equations (12) and (13) produce almost identical numerical results.

With the calculation of critical values, both JG and KE non-dimensionalized their interference, contact force and contact area as

$$\omega^* = \frac{\omega}{\omega_c} \tag{18}$$

$$P^* = \frac{P}{P_c} \tag{19}$$

$$A^* = \frac{A}{A_c} \tag{20}$$

where ω^*, P^* and A^* are the non-dimensional parameters of interference, contact force and contact area respectively. Values of ω^*, P^* and A^* equal to unity represent the onset of plastic deformation.

At large deformations, the contact hemisphere enters the fully plastic regime. The fully plastic regime was characterized by Johnson [**11**] as a state where the plastic strains are large compared with the elastic strains, which can be correlated to when the entire contact surface deforms plastically. Tabor [**12**] gave a similar definition and also provided a relationship of hardness to yield strength of $H \approx 3S_y$. Within the fully plastic regions, if strain hardening is small, the material will flow plastically at a constant stress, while conserving volume. The truncation model assumes that under fully plastic conditions the contact area of a hemisphere can be approximated by the truncation of the rigid sphere geometry by the rigid flat. The result is approximated as

$$A_P = 2\pi R\omega \tag{21}$$

The contact force on the hemisphere can be calculated as the contact area multiplied by the average pressure, which in the fully plastic regime is the hardness. The fully plastic contact force is given as

$$P_P = 2\pi R\omega H \tag{22}$$

where $H = 2.8S_y$, as previously stated. However, it was found by JG that this result is unsubstantiated. Greenwood and Tripp [**7**] also independently modelled fully plastic contact between hemispheres using a similar truncation method.